LIÈGE université
Sciences Appliquées

MATH0461-2 : INTRODUCTION TO NUMERICAL OPTIMIZATION

Project report

Compressed Sensing

Authors:
Maxime GALET (s170877)
Antoine DEBOR (s173215)

Lecturer:
Pr. Q. LOUVEAUX

Monday 7th December, 2020

1 Modelling

The different variables and matrices presented in the following and their corresponding domains are $r \in \mathbb{R}^N$, $\Phi \in \mathbb{R}^{M \times N}$, $m \in \mathbb{R}^M$ with $M < N$, $\Psi \in \mathbb{R}^{N \times N}$ and $x \in \mathbb{R}^N$. Prior to any development, let us recall the relationships between those different variables and matrices,

$$m = \Phi r$$

and

$$r = \Psi x.$$

From that, let us define $\Theta \in \mathbb{R}^{M \times N}$ such that

$$\Theta \equiv \Phi \Psi,$$

leading to the following relationship

$$m = \Theta x.$$

1.1

Using the ℓ_0 norm, the problem can be formulated as

$$\begin{aligned} \min \quad & \|x\|_0 \\ \text{s.t.} \quad & \Theta x - m = 0 \\ & x \in \mathbb{R}^N \end{aligned} \tag{1}$$

which is non convex since its objective function is not convex. The so called ℓ_0 norm is indeed not a convex function as it does not satisfy the Jensen inequality

$$\|\lambda x + (1-\lambda)y\|_0 \leq \lambda \|x\|_0 + (1-\lambda)\|y\|_0 \quad \text{for } \lambda \in [0,1], x, y \in \mathbb{R}^n. \tag{2}$$

Indeed, for $\lambda = \frac{1}{2}, x = (1,0)$ and $y = (0,1)$, the left-hand side is equal to 2 and the right-hand side is equal to 1, which violates the Jensen inequality.

1.2

Using the ℓ_1 norm, the problem can be formulated as

$$\begin{aligned} \min \quad & \|x\|_1 \\ \text{s.t.} \quad & \Theta x - m = 0 \\ & x \in \mathbb{R}^N \end{aligned} \tag{3}$$

which, through the epigraph trick, can be expressed as the following linear program

$$\begin{aligned} \min \quad & \sum_i t_i \\ \text{s.t.} \quad & -t_i < x_i < t_i \\ & \Theta x - m = 0 \\ & x \in \mathbb{R}^N, t \in \mathbb{R}^{N,+} \end{aligned} \tag{4}$$

where x_i represents the i^{th} element of the vector x. Instead of trying to minimize a sum of absolute values as defined by the ℓ_1 norm, which is not linear, this linear program seeks to minimize the sum of variables t_i, $i = 1, \ldots, N$, under the constraint that each element t_i provides an upper bound to the absolute value of each element x_i of x.

1.3

Using the ℓ_2 norm, the problem can be formulated as

$$\begin{aligned} \min \quad & \|x\|_2 \\ \text{s.t.} \quad & \Theta x - m = 0 \end{aligned} \tag{5}$$

which, using the epigraph trick again, equivalently writes

$$\begin{aligned} \min \quad & t \\ \text{s.t.} \quad & \|x\|_2 < t \\ & \Theta x - m = 0 \\ & x \in \mathbb{R}^N, t \in \mathbb{R}^+. \end{aligned} \tag{6}$$

This program can eventually be expressed as the following second-order cone program

$$\begin{aligned} \min \quad & t \\ \text{s.t.} \quad & x \in \mathbb{L}^{N+1} = \{\|x\|_2^2 < t^2, t \geq 0\} \\ & \Theta x - m = 0 \\ & x \in \mathbb{R}^N, t \in \mathbb{R}^+, \end{aligned} \tag{7}$$

since the constraint $\|x\|_2 = \sqrt{\sum_{i=1}^N x_i^2} < t$ is equivalent[1] to $\|x\|_2^2 < t^2$.

1.4

In order to provide a closed-form solution to the ℓ_2 norm problem, one can first note that a vector x solution of the original objective function

$$\min \|x\|_2$$

is equivalent to a vector x solution of

$$\min \|x\|_2^2,$$

since the square function is strictly increasing on $\mathbb{R}^+$. The remaining problem is convex since its objective function is convex[2] and its equality constraint is linear. The Lagrange function of the new problem then writes

$$\mathcal{L}(x, \lambda) = \|x\|_2^2 - \lambda(\Theta x - m), \tag{8}$$

with the new variable λ as the Lagrange multiplier. One can now solve

$$\nabla_{x,\lambda} \mathcal{L}(x, \lambda) = 0 \tag{9}$$

to find a stationary point (x^*, λ^*) of the Lagrange function. This equation yields

$$\nabla_x \mathcal{L} = 0 \iff 2x - (\lambda\Theta)^T = 0 \tag{10}$$

and

$$\nabla_\lambda \mathcal{L} = 0 \iff \Theta x - m = 0. \tag{11}$$

According to equation 11, a vector x^* corresponding to a stationary point of the Lagrange function is given by

$$\begin{aligned} & \Theta x^* = m \\ \iff & \Theta^T \Theta x^* = \Theta^T m \\ \iff & (\Theta^T\Theta)^{-1}(\Theta^T\Theta)x^* = (\Theta^T\Theta)^{-1}\Theta^T m \\ \iff & x^* = (\Theta^T\Theta)^{-1}\Theta^T m = \Theta^T(\Theta\Theta^T)^{-1} m. \end{aligned} \tag{12}$$

[1] Since the square root function is strictly increasing on its domain.

[2] The ℓ_2 norm is convex since it is a norm and the square function is convex and strictly increasing on $[0; +\infty[$, therefore the square of the ℓ_2 norm is convex.

The condition $\nabla_{x,\lambda}\mathcal{L}(x,\lambda) = 0$ is actually equivalent to the Karush-Kuhn-Tucker conditions in the considered problem, which is a necessary condition for x^* to be a local minimum. Indeed, since the only constraint of the considered convex problem is an equality, there is no need to consider the complementarity slackness condition. Furthermore, the primal feasibility is ensured since condition 11 is the same as the constraint of the primal problem. Finally, the dual feasibility is also ensured since the fact that the primal constraint is an equality implies a free dual variable, meaning no restriction on the feasible set of the dual variable.

In the case of a convex problem, Karush-Kuhn-Tucker conditions are sufficient to say that x^* is a local minimum of the objective function. Furthermore, every local minimum is a global one for a convex problem. Therefore, one can deduce that x^* is a closed-form solution of the considered problem.

In addition to that, it is worth noting that the considered problem is *strongly* convex, which implies that x^* is actually unique. Indeed, its objective function $f(x) = \|x\|_2^2$ is *strongly* convex with parameter $m > 0$ since, for every x and y on its domain, it satisfies the following inequality

$$\begin{aligned} &(\nabla f(x) - \nabla f(y))^T (x-y) \geq m\|x-y\|_2^2 \\ \iff &(2x-2y)^T(x-y) \geq m\|x-y\|_2^2 \\ \iff &2(x-y)^T(x-y) \geq m\|x-y\|_2^2 \\ \iff &2\|x-y\|_2^2 \geq m\|x-y\|_2^2, \end{aligned} \tag{13}$$

for $0 < m \leq 2$.

One can notice that x^* is defined only if $\Theta\Theta^T$ has full rank, that is to say if[3] $rank(\Theta\Theta^T) = M$. Since for a real matrix A, one has that $rank(AA^T) = rank(A)$, the condition on Θ for x^* to exist is $rank(\Theta) = M$. As Θ is $M \times N$, $rank(\Theta) \leq \min\{M, N\} = M$ and the condition on Θ for x^* to exist corresponds thus to Θ having full rank.
Since Ψ is orthogonal and thus full rank, the Sylvester inequality stands that

$$\begin{aligned} &rank(\Phi) + rank(\Psi) - N \leq rank(\Theta) \\ \iff &rank(\Phi) + N - N \leq rank(\Theta) \\ \iff &rank(\Phi) \leq rank(\Theta), \end{aligned} \tag{14}$$

and a way to ensure that Θ has full rank is thus to impose that Φ has also full rank. This condition on Φ corresponds to not having redundancy in the acquisition of data and that each new sample brings information that can not be expressed on the basis of the previous measurements.

1.5

One can formulate the three following variants of the ℓ_1-norm problem. The first one writes

$$\begin{aligned} \min \quad & \|x\|_1 \\ \text{s.t.} \quad & \|\Theta x - m\|_2 \leq \epsilon \\ & x \in \mathbb{R}^N, \end{aligned} \tag{15}$$

which can be equivalently re-written as the following SOC program

$$\begin{aligned} \min \quad & \sum_i t_i \\ \text{s.t.} \quad & -t_i < x_i < t_i \\ & \|\Theta x - m\|_2^2 \leq \epsilon^2 \\ & x \in \mathbb{R}^N, t \in \mathbb{R}^{N,+}, \end{aligned} \tag{16}$$

[3] Since $\Theta\Theta^T$ is $M \times M$.

using the epigraph trick, and the second one writes

$$\begin{aligned} \min \quad & \|x\|_1 + \lambda \|\Theta x - m\|_2 \\ \text{s.t.} \quad & x \in \mathbb{R}^N, \end{aligned} \tag{17}$$

which can also be equivalently re-written as the following SOC program

$$\begin{aligned} \min \quad & \sum_i \mu_i + \lambda \nu \\ \text{s.t.} \quad & -\mu_i \leq x_i \leq \mu_i, \quad \text{for } i = 1, \dots, N \\ & \|\Theta x - m\|_2^2 \leq \nu^2 \\ & x \in \mathbb{R}^N, \mu \in \mathbb{R}^{N,+}, \nu \in \mathbb{R}^+ \end{aligned} \tag{18}$$

using the epigraph trick again. Both problems are more relaxed in term of constraints as the reconstructed signal may not exactly match the measurements up to some tolerance, explicitly given as $\epsilon \in \mathbb{R}^+$ in the first variant, and implicitly hidden behind $\lambda \in \mathbb{R}_0^+$ in the second one[4]. These variants are thus expected to be more robust against noisy measurements, as a zero tolerance yields a perfect match with noise, which is not wanted.

The third one is a variant of the first one and can be written as

$$\begin{aligned} \min \quad & \|x\|_1 \\ \text{s.t.} \quad & (\Theta x - m)_j \leq \epsilon, \quad \text{for } j = 1, \dots, M \\ & x \in \mathbb{R}^N, \end{aligned} \tag{19}$$

which can be equivalently re-written as

$$\begin{aligned} \min \quad & \sum_i t_i \\ \text{s.t.} \quad & -t_i < x_i < t_i \\ & (\Theta x - m)_j \leq \epsilon \\ & x \in \mathbb{R}^N, t \in \mathbb{R}^{N,+}. \end{aligned} \tag{20}$$

Note that the equality constraint as formulated here is not strictly equivalent to constraining the infinity norm of $\Theta x - m$ to be lower than ϵ as one do not consider the absolute value of each element $(\Theta x - m)_j$.

2 Numerical experiments

2.1

The implementation of the different formulations derived in the previous sections can be found in the Julia scripts of the provided archive. The original ℓ_1 and ℓ_2 problems are coded up in files `[L1-uncorrupted/noisy].jl` and `[L2-uncorrupted/noisy].jl` respectively, while the three variants depicted in section 1.5 can be found in `[L1-var1].jl`, `[L1-var2].jl` and `[L1-var3].jl`.

In order to judge the performance of these different methods, the reconstructed images will be compared to the 78×78 pixels original one, shown in figure 1.

[4] λ actually penalizes mismatches between the reconstructed signal and the measurements. The larger the value of λ, the stronger the penalization, and the closest to each other the reconstructed signal and the measurements.

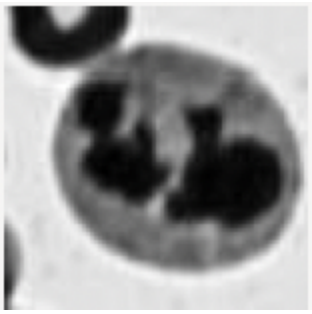

Figure 1: Original grayscale cell image

Note that, in order to save the different reconstructed grayscale images as `PNG` files, the corresponding computed matrices have been post-processed to contract their elements between 0 and 1[5].

2.2

Solving the ℓ_1 and ℓ_2 problems numerically for the set of uncorrupted measurements with Julia provides different reconstructed images which can be seen in figures 2 and 3 respectively. One can compare the performance of both methods for different number of measurements by comparing these reconstructed images with the original grayscale image shown in figure 1.

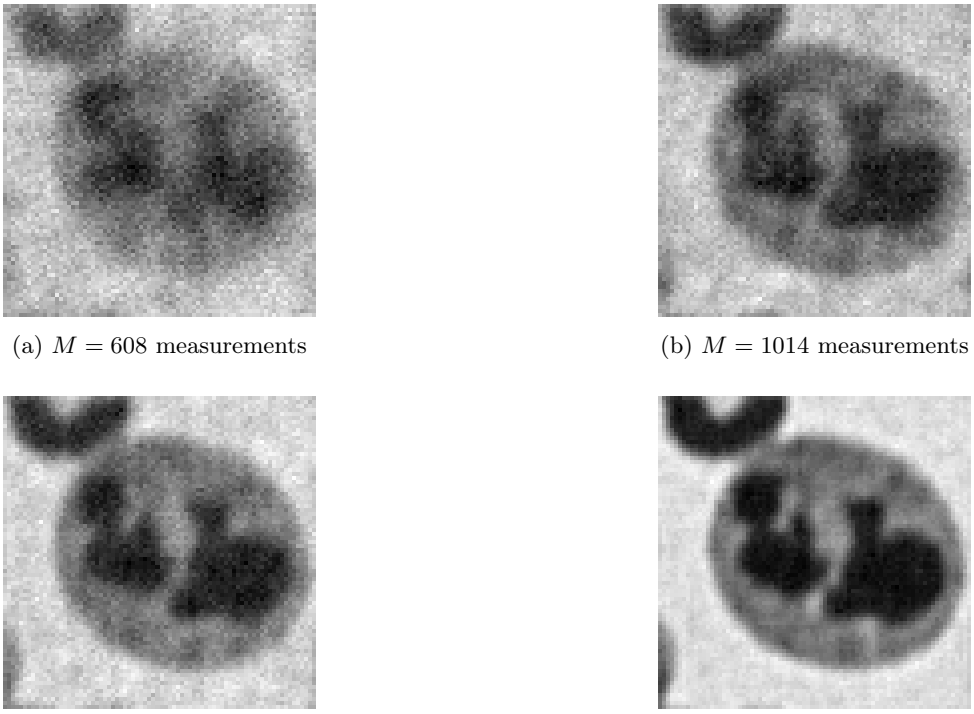

(a) $M = 608$ measurements

(b) $M = 1014$ measurements

(c) $M = 1521$ measurements

(d) $M = 3042$ measurements

Figure 2: Reconstructed grayscale images from uncorrupted mesurements for the ℓ_1-norm problem

One can see from figure 2 that solving the ℓ_1-norm problem provides optimal (approximately) sparse vectors $\hat{x}$ leading to quite faithful reconstructions of the cell image. Indeed, while the global quality of the image logically increases with the number of measurements, one can observe that even for $M = 1014$, which

[5]Element e_i of vector E is replaced by e_i'' such that $e_i' = e_i - \min_{e_j \in E}(e_j)$ and $e_i'' = \frac{e_i'}{\max_{e_j' \in E'}(e_j')}$.

corresponds to $\frac{1}{6}$ of the total number of pixels of the original image, the reconstruction enables to quite clearly distinguish the different zones of the image. For $M = 608$, however, the quality obtained may be too poor to carry out analyses for instance, since one observes poor contrast and resolution. These conclusions obviously depend on the context in which these images are to be used.

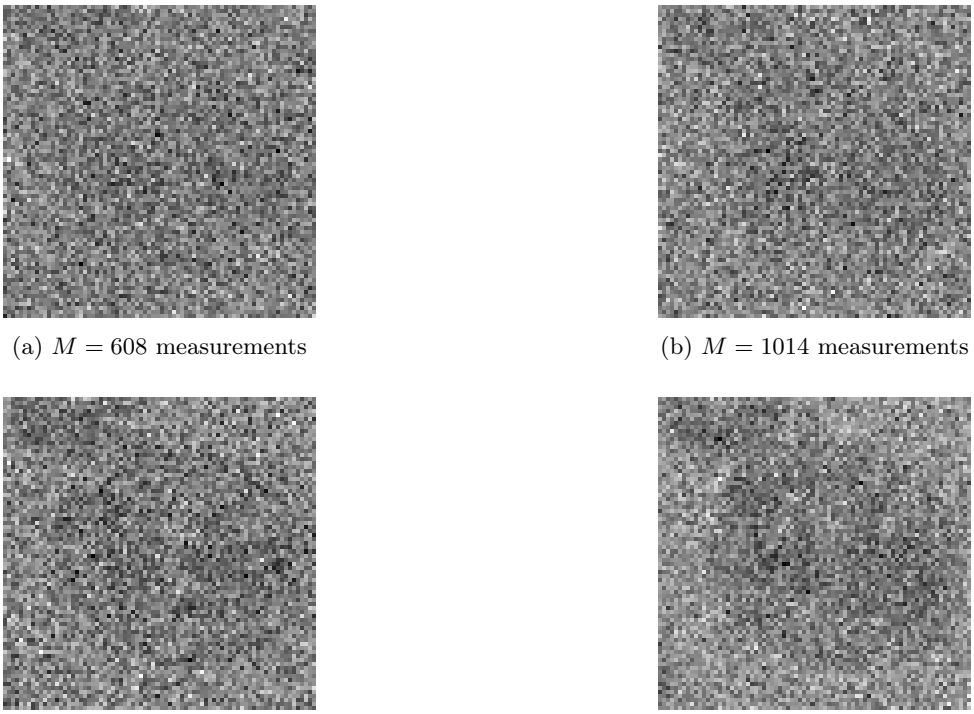

(a) $M = 608$ measurements

(b) $M = 1014$ measurements

(c) $M = 1521$ measurements

(d) $M = 3042$ measurements

Figure 3: Reconstructed grayscale images from uncorrupted mesurements for the ℓ_2-norm problem

In contrast with the ℓ_1-norm, one can see from figure 3 that solving the ℓ_2-norm problem provides solutions for x leading to poor reconstructions of the cell image in terms of quality. This time, even for $M = 3042$, which corresponds to $\frac{1}{2}$ of the total number of pixels of the original image, the reconstruction does not enable to clearly distinguish the different zones of the cell. Actually, except maybe for $M = 3042$, it might be quite impossible to guess the global content of the original image without seeing it beforehand. This method can thus not be used to generate images for analysis on the basis of few measurements. However, it can again be observed that there is a slight but logical improvement in quality for increasing values of M, as one can better and better guess the shape of the cell in the image.

The difference between the results obtained by solving the ℓ_1-norm problem and those obtained by solving the ℓ_2-norm problem is directly related to the sparsity of the solution. Indeed, the ℓ_1-norm is capable of producing a sparser solution which, in the scope of compressed sensing, induces a more precise solution. This is illustrated in figure 4, representing the ℓ_1-norm and ℓ_2-norm 2D geometric representations, for a vector $w = (x_1, x_2)$ defined in the 2D space.

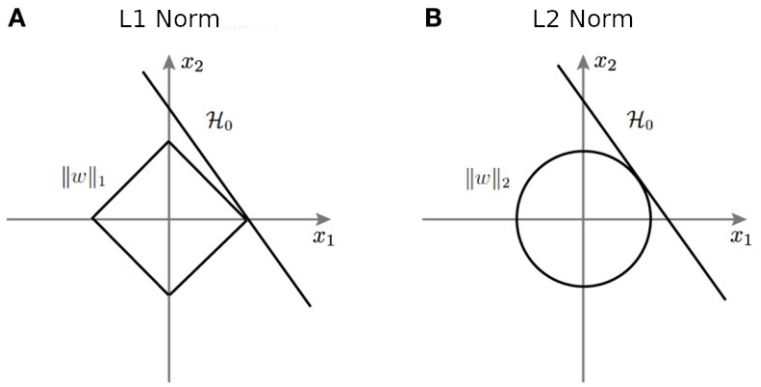

Figure 4: Comparison of the geometry for the ℓ_1-norm and the ℓ_2-norm

The solution for the minimization of the ℓ_1-norm (i.e the intersection between the diamond and $\mathcal{H}_0$, a set related to an equality constraint) yields a zero value for x_2 and a non-zero value for x_1. In contrast, due to the "ball" geometry of the ℓ_2-norm, the solution for the latter is a combination of non-zero values of x_1 and x_2, which shows that this method does not promote sparse solutions.

2.3

A dual variable can in general be seen as the marginal cost upon the objective function at optimality caused by a (small) variation of the corresponding constraint; more precisely, it quantifies how much the primal objective function increases when the right hand side of the constraint is increased by 1.
Considering the ℓ_1-norm problem provided in section 1.3, one could consider that there is only one equality constraint, namely

$$\Theta x - m = 0 \iff \Theta x = m.$$

In this particular case, the dual variable associated with this equality constraint quantifies in a way how the ℓ_1-norm of x will be modified if the right-hand side of the equality, that is m, is modified. In other words, the dual variable can be interpreted as a measure of the impact of noise, which will modify the measurement matrix m from its initial uncorrupted value, on the ℓ_1-norm of x, hence on the sparsity of the latter.

Actually, there is one equality constraint for each element of $\Theta x - m$, but, considering the multi-dimensional object x as the variable of the optimization problem, one has considered its related equality constraint as a unique one for the sake of the interpretation. If one now consider one equality constraint for each element of $\Theta x - m$, each related dual variable quantifies how the objective function will be impacted by a change in the related element of m, that is by a noisy measurement.

One can also look at the range over which these dual variables are relevant. This range tells how much the right-hand side coefficients can change (i.e how much noise can be added to measurements) before the basis changes and the dual variables no longer can be interpreted as before. Actually, when the basis changes, the set of tight constraints is not the same anymore, meaning that some non zero valued dual variables become zero and the other way around. This means that the previous values of the dual variables do not gives any information anymore about change in the optimal function value due to noise presence. This can be observed in the following graph, where the aforementioned range is plotted for every equality constraint linked to the uncorrupted measurement vector of size 608. The blue dots correspond to the lower bound of the interval, and the orange ones to the upper bound.

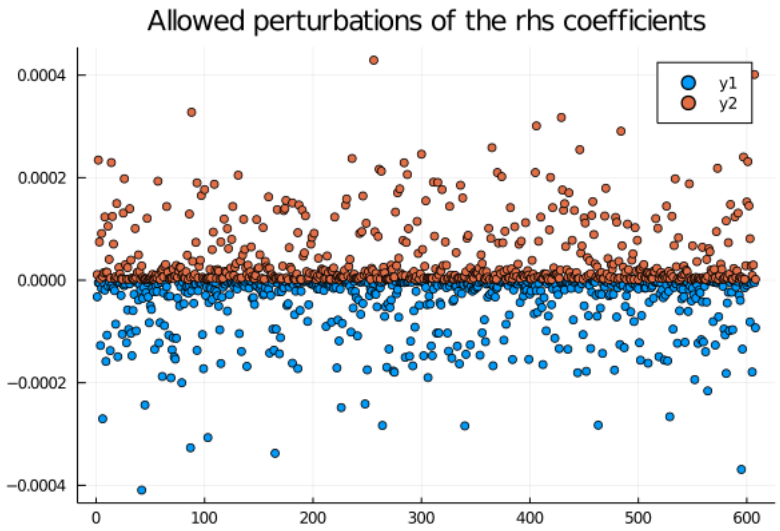

One can see that the allowed intervals are incredibly small, with most of them being close to empty (with a consequent, albeit relatively small number of outliers). This means that the computation based on the ℓ_1-norm is highly sensitive to a noisy input.

2.4

Solving the original ℓ_1 problem numerically for the set of noisy measurements with Julia provides differents reconstructed images which can be seen in figure 5. Once can analyze the performance of this method for different number of noisy measurements by again comparing these reconstructed images with the original grayscale image shown in figure 1.

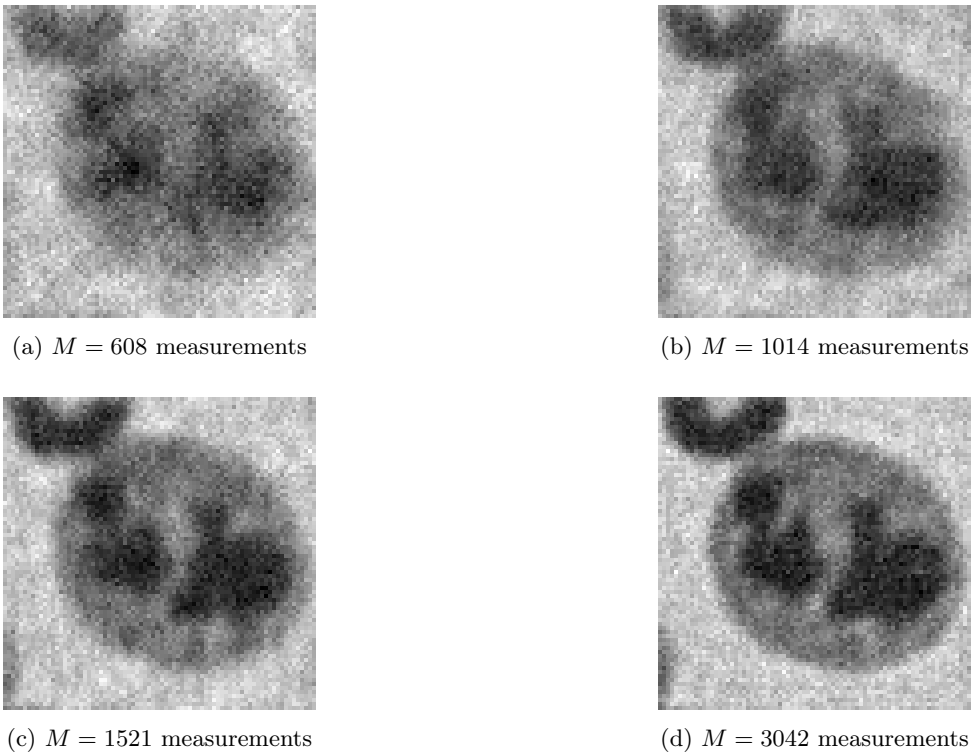

(a) $M = 608$ measurements

(b) $M = 1014$ measurements

(c) $M = 1521$ measurements

(d) $M = 3042$ measurements

Figure 5: Grayscale reconstruction images from noisy mesurements with ℓ_1-norm problem

From figure 5, one can observe that even for noisy measurements, the performance of the ℓ_1-norm method is way better than what has been previously observed for the ℓ_2-norm method with uncorrupted measurements. Although logically providing less contrast and resolution than with uncorrupted measurements, this method provides quite faithful reconstructions of the original image. Again, the quality obtained for $M = 608$ may be too week for analysis as it presents poor resolution.

The original ℓ_1-norm problem does not, however, take into account the possible presence of noise in measurements. Three variants have thus be presented in section 1.5, whose intended purpose is to provide enhanced robustness against noisy measurements, eventually leading to more contrast. Solving these three variants[6] numerically for the set of noisy measurements and for different values of ϵ and λ provide reconstructed images of variable quality. One can find numerous hyper parameters tuning trials and further analyses about these parameters in the appendix A, while (close to) optimal results are presented and compared to the original image and the non robust ℓ_1-norm results in figures 6 to 17.

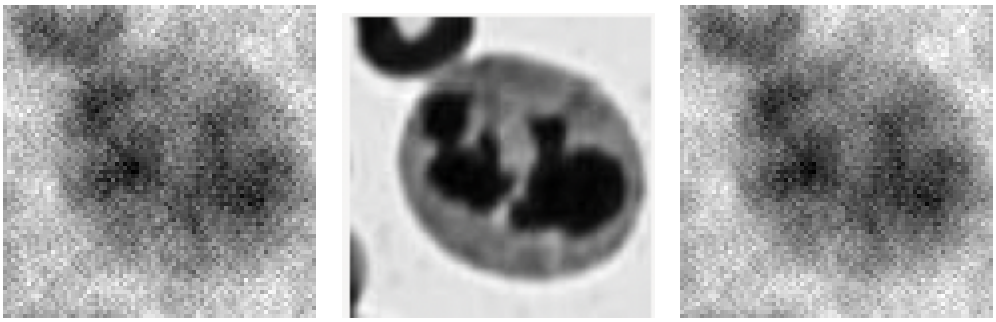

(a) Original ℓ_1-norm (b) Original (c) $\epsilon = 0.1$

Figure 6: First variant, for $M = 608$

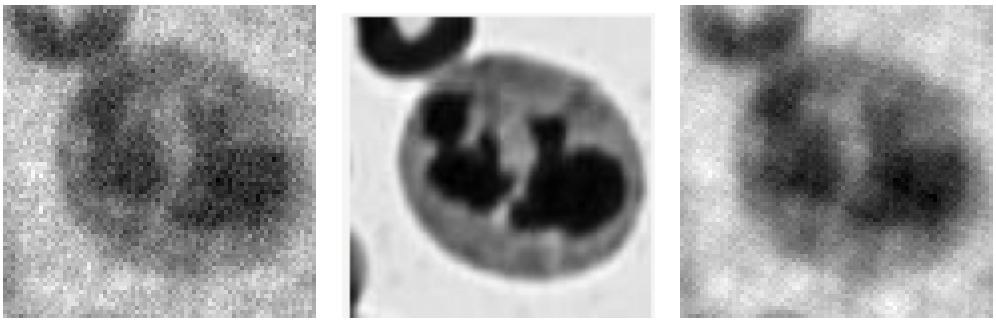

(a) Original ℓ_1-norm (b) Original (c) $\epsilon = 0.2$

Figure 7: First variant, for $M = 1014$

[6]See 16, 18 and 20.

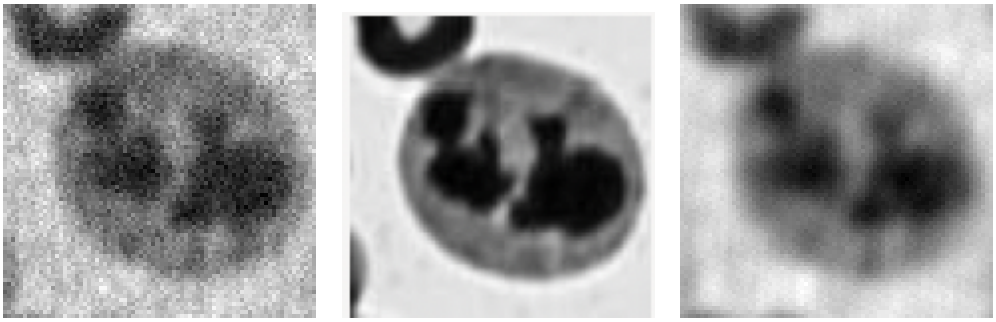

(a) Original ℓ_1-norm (b) Original (c) $\epsilon = 0.2$

Figure 8: First variant, for $M = 1521$

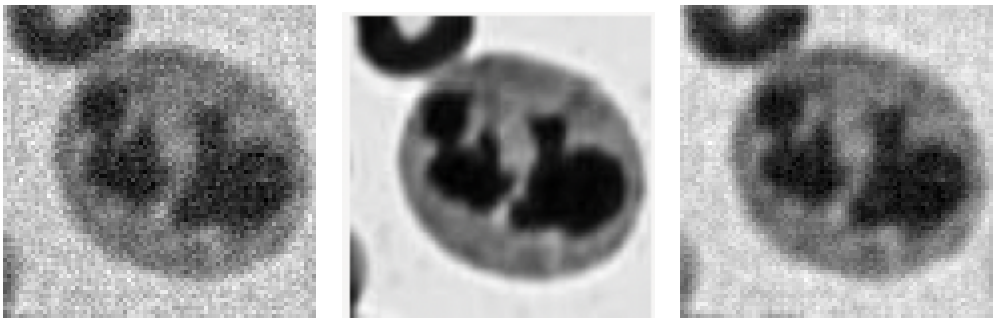

(a) Original ℓ_1-norm (b) Original (c) $\epsilon = 0.05$

Figure 9: First variant, for $M = 3042$

From figures 6 to 9, one can see that, provided that a good[7] value of the hyper parameter ϵ is chosen, the first variant can provide reconstructed images providing more contrast than the original ℓ_1-norm method, hence showing more robustness against noisy measurements. This phenomenon might appear less obvious for low values of M, but one can still notice small regions wither or blacker than for the original ℓ_1-norm method, alongside a logically lower accuracy due to the small quantity of measurements.

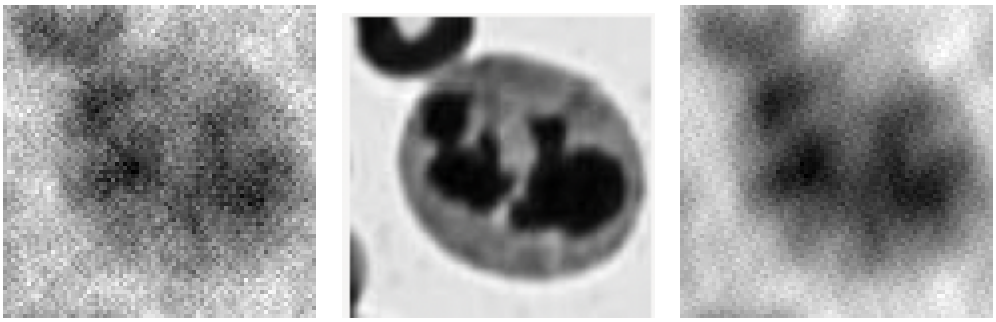

(a) Original ℓ_1-norm (b) Original (c) $\lambda = 250$

Figure 10: Second variant, for $M = 608$

[7]The presented value is the result of a tuning process, please see the appendix A for trials.

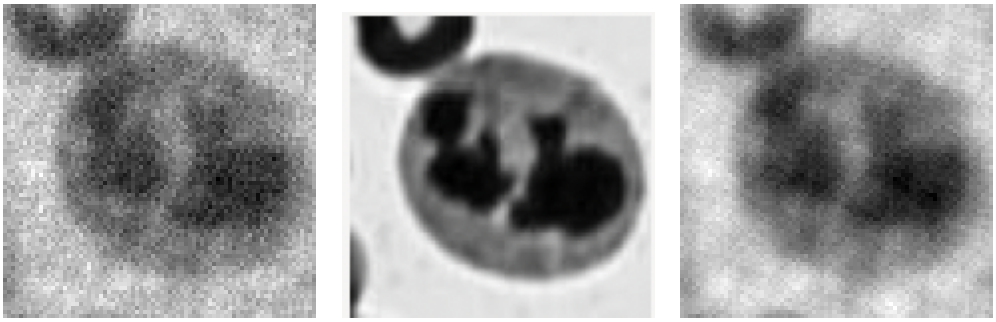

(a) Original ℓ_1-norm (b) Original (c) $\lambda = 500$

Figure 11: Second variant, for $M = 1014$

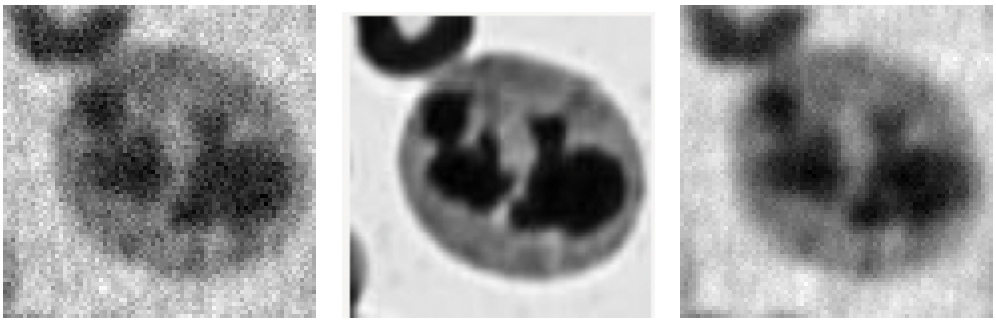

(a) Original ℓ_1-norm (b) Original (c) $\lambda = 750$

Figure 12: Second variant, for $M = 1521$

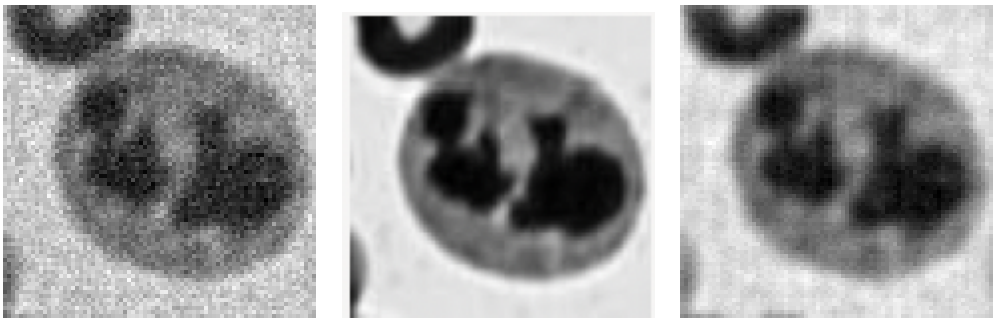

(a) Original ℓ_1-norm (b) Original (c) $\lambda = 1750$

Figure 13: Second variant, for $M = 3042$

From figures 10 to 13, one can see that the second variant, just like the first one, shows a enhanced robustness against noisy measurements compared to the original ℓ_1-norm method. It again requires tuning for the hyper parameter λ and leads to quite faithful reconstructions, especially in term of contrast. For low values of M like $M = 608$, again, the method logically does however not provide great accuracy.

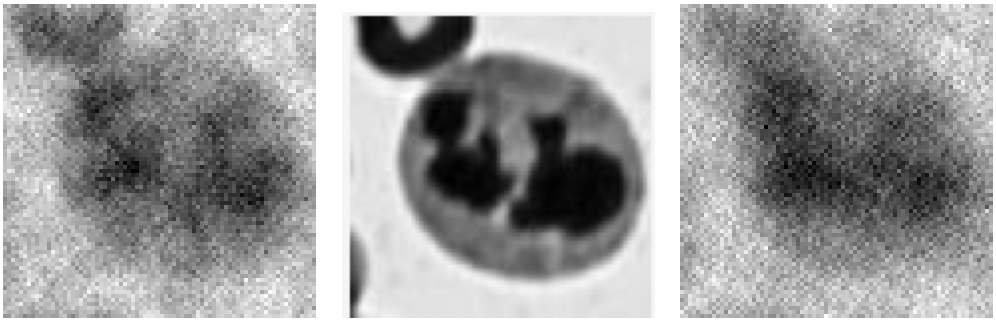

(a) Original ℓ_1-norm (b) Original (c) $\epsilon = 0.005$

Figure 14: Third variant, for $M = 608$

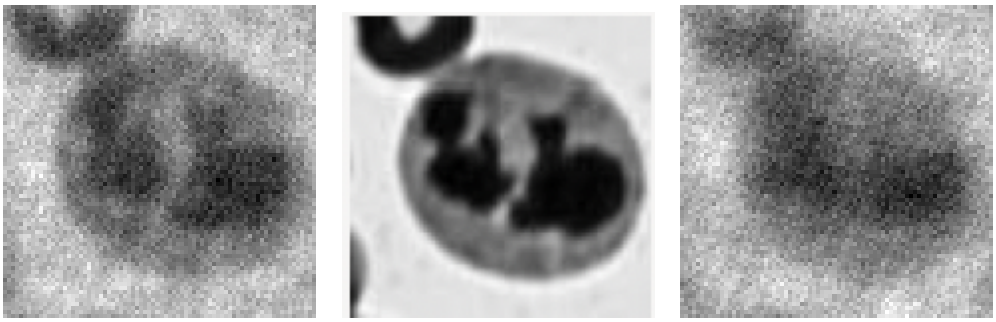

(a) Original ℓ_1-norm (b) Original (c) $\epsilon = 0.005$

Figure 15: Third variant, for $M = 1014$

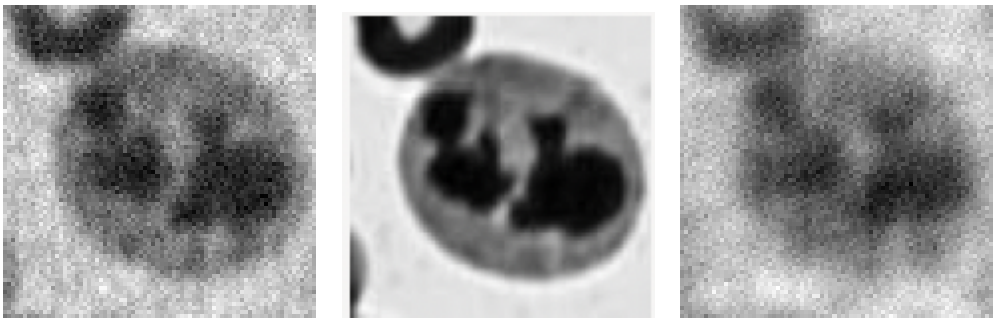

(a) Original ℓ_1-norm (b) Original (c) $\epsilon = 0.005$

Figure 16: Third variant, for $M = 1521$

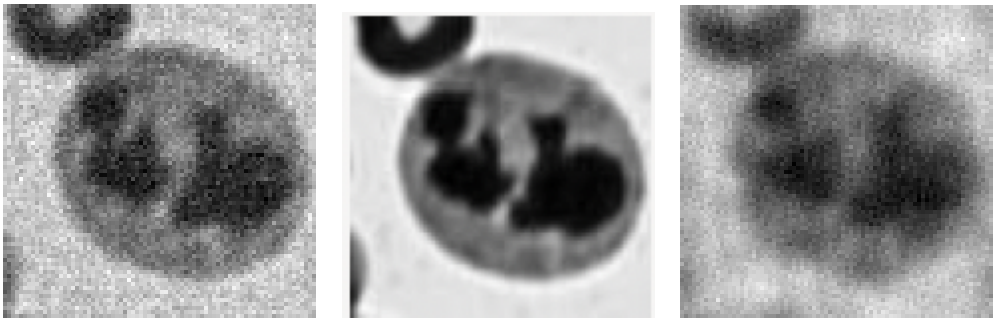

(a) Original ℓ_1-norm (b) Original (c) $\epsilon = 0.003$

Figure 17: Third variant, for $M = 3042$

From figures 14 to 17, one can observe that the third variant provides poorer results than the two first ones, especially for low values of M. Actually, the low gain in contrast comparing to the original ℓ_1-norm is counterbalanced by a quite low accuracy, even for $M = 3042$. One can thus not use this method to gather faithful reconstructions with enhanced robustness against noisy measurements.

Appendix A Reconstructed images for proposed variants

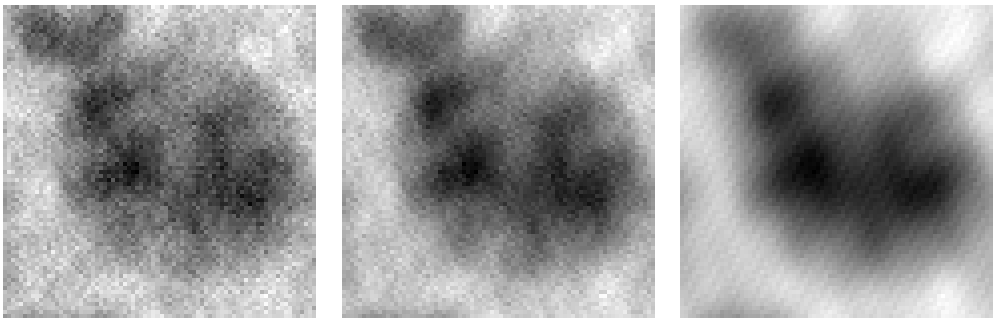

(a) $\epsilon = 0.1$ (b) $\epsilon = 0.3$ (c) $\epsilon = 0.5$

Figure 18: First variant, for $M = 608$

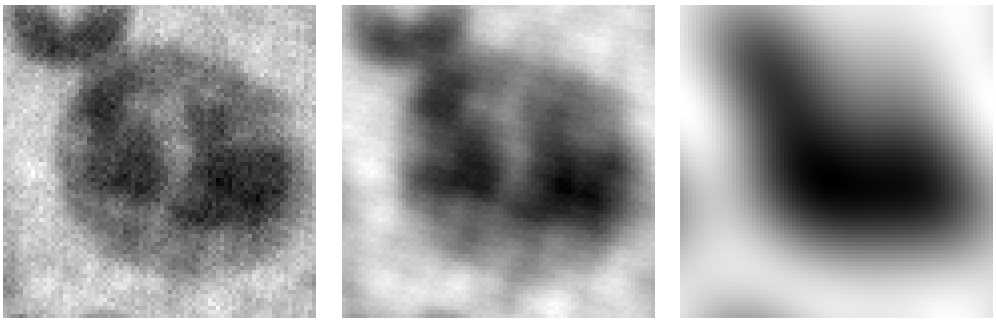

(a) $\epsilon = 0.1$ (b) $\epsilon = 0.3$ (c) $\epsilon = 0.5$

Figure 19: First variant, for $M = 1014$

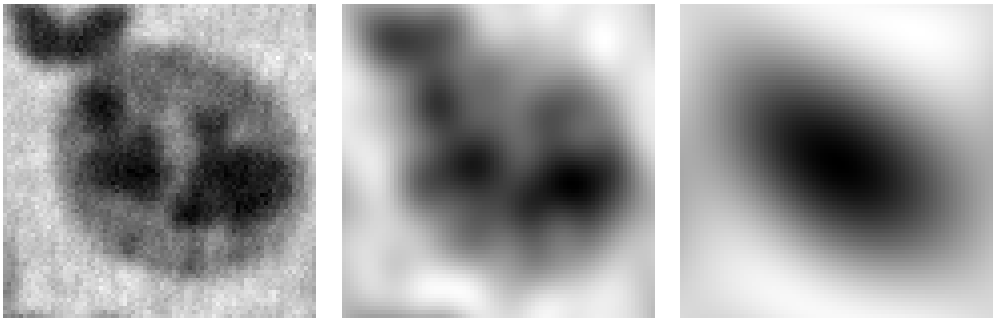

(a) $\epsilon = 0.1$ (b) $\epsilon = 0.3$ (c) $\epsilon = 0.5$

Figure 20: First variant, for $M = 1521$

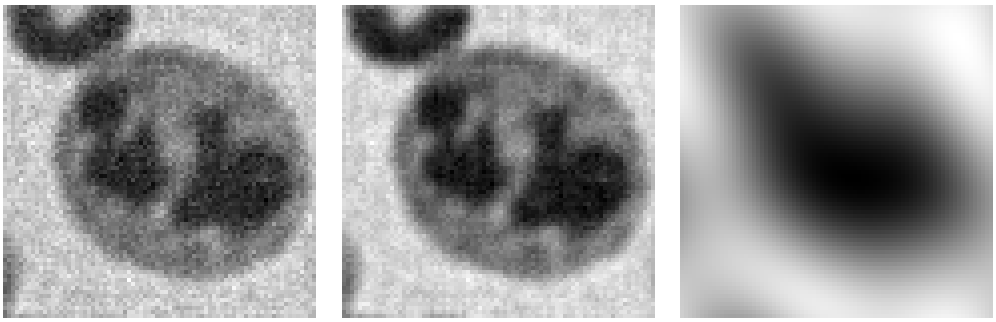

(a) $\epsilon = 0.01$ (b) $\epsilon = 0.05$ (c) $\epsilon = 0.3$

Figure 21: First variant, for $M = 3042$

From figures 18 to 21, one can observe that, for a small enough value of ϵ, solving the first variant allows to obtain reconstructed images quite similar to what has been obtained with the original method, while providing more contrast in some cases. The accuracy of the results obtained with this method obviously relies on the value of ϵ, and setting this tolerance to a too large value leads to pretty bad results as it can be seen in figures 18c, 19c, 20c and 21c. Indeed, a large tolerance does not constraint enough the reconstructed image to match the measurements. However, setting ϵ to a too small value is close to the original problem, and it does not take into account the presence of noise. An intermediate value can thus be sought in order to combine accuracy and contrast.

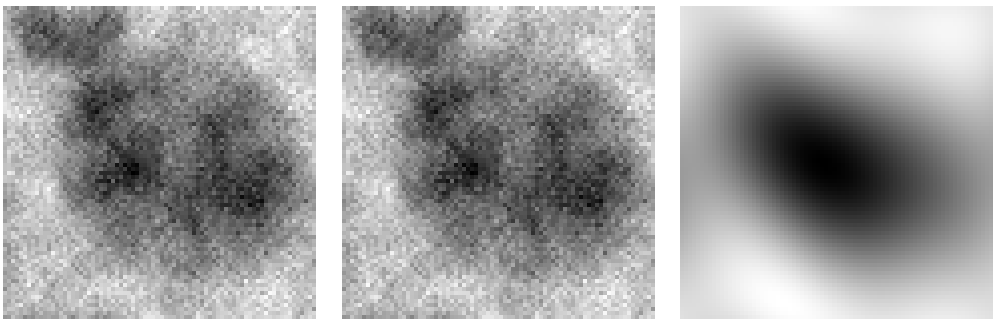

(a) $\lambda = 10000$ (b) $\lambda = 1000$ (c) $\lambda = 100$

Figure 22: Second variant, for $M = 608$

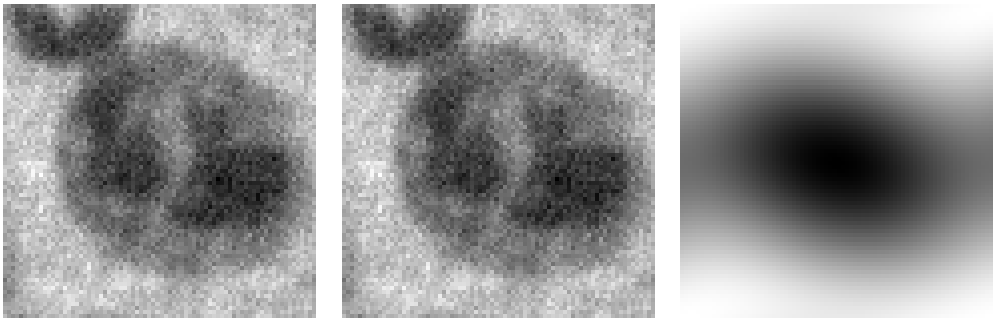

(a) $\lambda = 10000$ (b) $\lambda = 1000$ (c) $\lambda = 100$

Figure 23: Second variant, for $M = 1014$

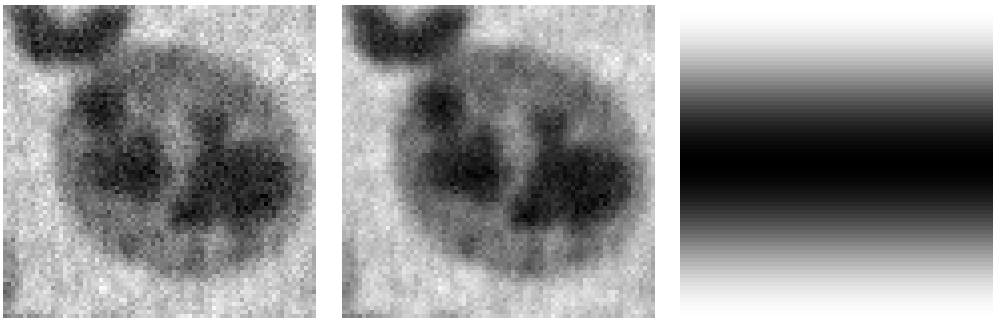

(a) $\lambda = 10000$ (b) $\lambda = 1000$ (c) $\lambda = 100$

Figure 24: Second variant, for $M = 1521$

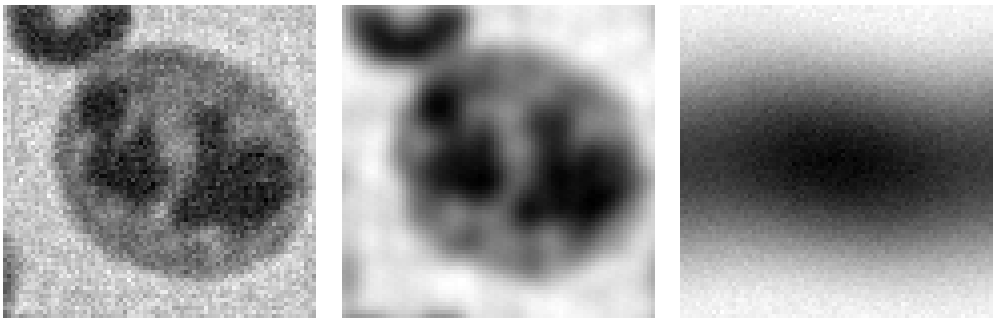

(a) $\lambda = 10000$ (b) $\lambda = 1000$ (c) $\lambda = 100$

Figure 25: Second variant, for $M = 3042$

From figures 22 to 25, one can see that the second variant also provides valuable results for pertinent values of the penalization factor λ. Indeed, this factor has to be large enough in order for the match between reconstruction and measurements to have sufficient weight in the objective function. As it can be seen in figures 22c, 23c, 24c and 25c, setting a too small value for λ provides inoperative results. In contrast, setting a too high value of the hyper parameter yields no robustness against noise, and, again, a trade-off has to be sought to provide sufficient contrast and accuracy.

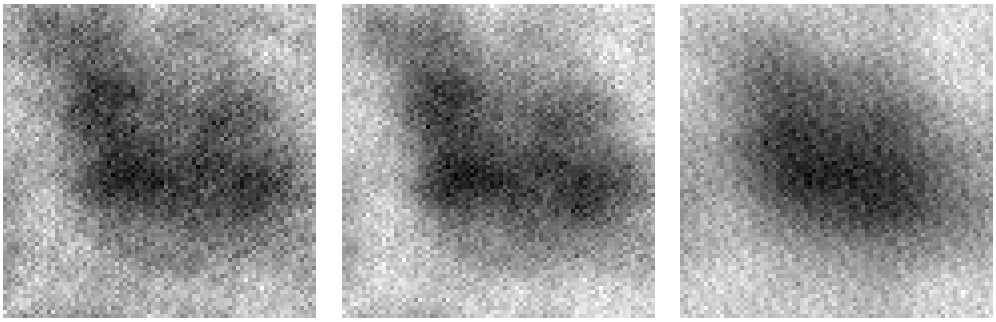

(a) $\epsilon = 0.001$ (b) $\epsilon = 0.01$ (c) $\epsilon = 0.03$

Figure 26: Third variant, for $M = 608$

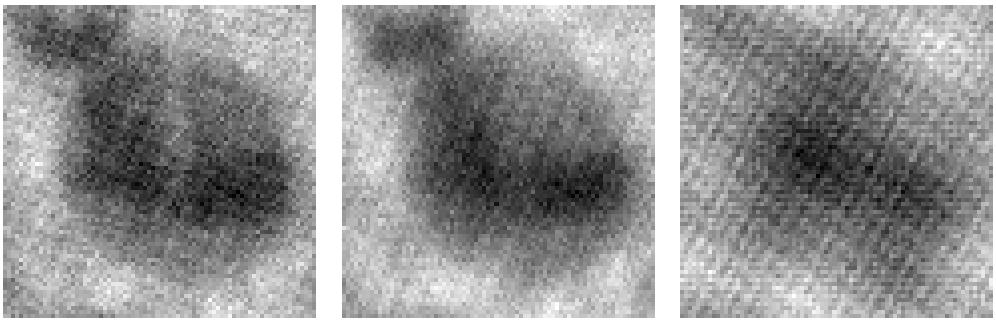

(a) $\epsilon = 0.001$ (b) $\epsilon = 0.01$ (c) $\epsilon = 0.03$

Figure 27: Third variant, for $M = 1014$

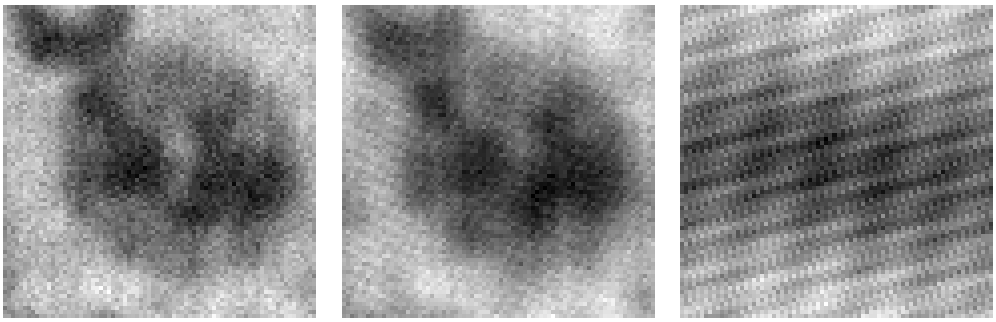

(a) $\epsilon = 0.001$ (b) $\epsilon = 0.01$ (c) $\epsilon = 0.03$

Figure 28: Third variant, for $M = 1521$

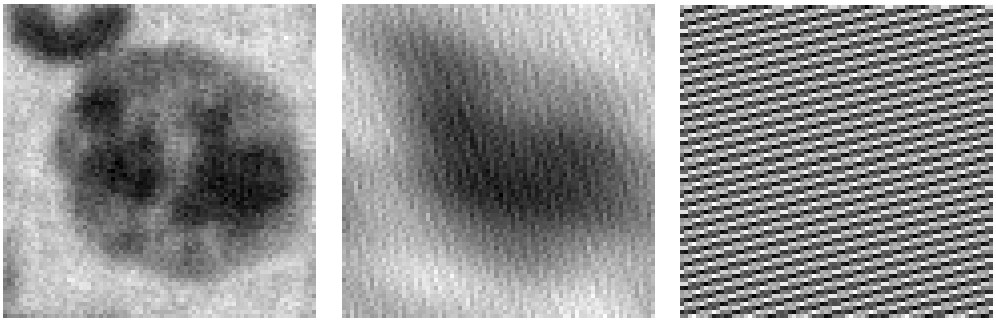

(a) $\epsilon = 0.001$ (b) $\epsilon = 0.01$ (c) $\epsilon = 0.03$

Figure 29: Third variant, for $M = 3042$

From figures 26 to 29, one can observe that the third variant never provides results really better than the original ℓ_1-norm method. Yet sometimes providing more contrast, the reconstructed images are not as accurate and contain artefacts. While still better for some values of ϵ than what has been observed solving the ℓ_2-norm problem for uncorrupted measurements, this method does not provide quality reconstructions. One can however note that for $M = 3042$ and a tolerance $\epsilon = 0.001$, the reconstructed image of figure 29a still presents a resolution allowing the identification of the different parts of the cell without too much ambiguity, but with poor contrast.